

VIROLOGY

Subtle differences in the pathogenicity of SARS-CoV-2 variants of concern B.1.1.7 and B.1.351 in rhesus macaques

Vincent J. Munster¹, Meaghan Flagg¹, Manmeet Singh¹, Claude Kwe Yinda¹, Brandi N. Williamson¹, Friederike Feldmann², Lizzette Pérez-Pérez¹, Jonathan Schulz¹, Beniah Brumbaugh¹, Myndi G. Holbrook¹, Danielle R. Adney¹, Atsushi Okumura¹, Patrick W. Hanley², Brian J. Smith², Jamie Lovaglio², Sarah L. Anzick³, Craig Martens³, Neeltje van Doremalen¹, Greg Saturday², Emmie de Wit^{1*}

The emergence of several SARS-CoV-2 variants has caused global concerns about increased transmissibility, increased pathogenicity, and decreased efficacy of medical countermeasures. Animal models can be used to assess phenotypical changes in the absence of confounding factors. Here, we compared variants of concern (VOC) B.1.1.7 and B.1.351 to a recent B.1 SARS-CoV-2 isolate containing the D614G spike substitution in the rhesus macaque model. B.1.1.7 behaved similarly to D614G with respect to clinical disease and replication in the respiratory tract. Inoculation with B.1.351 resulted in lower clinical scores, lower lung virus titers, and less severe lung lesions. In bronchoalveolar lavages, cytokines and chemokines were up-regulated on day 4 in animals inoculated with D614G and B.1.1.7 but not with B.1.351. In nasal samples, cytokines and chemokines were up-regulated only in the B.1.1.7-inoculated animals. Together, our study suggests that circulation under diverse evolutionary pressures favors transmissibility and immune evasion rather than increased pathogenicity.

INTRODUCTION

As the COVID-19 pandemic continues, so does the evolution of SARS-CoV-2 in the still relatively susceptible global population. The detection of the B.1.1.7 variant in the United Kingdom prompted the World Health Organization to institute a classification system for new variants, with variants of concern (VOC) displaying increased transmissibility or detrimental changes in COVID-19 epidemiology; increased virulence or a change in clinical disease presentation; or decreased effectiveness of public health and social measures, or available diagnostics, vaccines, or therapeutics (1). B.1.1.7 and B.1.351 were the first variants to be designated VOC. After initial detection, both variants spread to many other countries, fueling concerns about their transmissibility and the efficacy of vaccines. As more epidemiological data on human cases of B.1.1.7 infection become available, it appears that this variant transmits more efficiently than the variants it displaced (2–6), possibly because of increased virus shedding (7). Whether there is an increased disease severity associated with B.1.1.7 infection remains unclear (4, 8–11). Data on infection in humans with B.1.351 are not yet widely available, and although its rapid spread suggests increased transmissibility, there are no data to confirm this (12–14). Similar to B.1.1.7, it is not clear whether B.1.351 infections are associated with a change in pathogenicity compared with the other circulating SARS-CoV-2 viruses (12–14).

Epidemiological data on increased transmissibility and disease severity can be confounded by changes in human behavior and an

increased number of cases affecting patient care. Although animal models do not completely recapitulate human disease, they are useful tools to assess several phenotypical changes such as virus transmission and pathogenesis in the absence of confounding factors. Several studies of the B.1.1.7 and B.1.351 variants in hamsters have been completed (15–17). However, since the changes in the spike receptor binding domain present in these variants could affect binding to the human versus hamster angiotensin-converting enzyme 2 (ACE2) differently, the replication kinetics of B.1.1.7 and B.1.351 may differ between hamsters and humans. The rhesus macaque is a widely used model of SARS-CoV-2 infection (18), and the amino acids in ACE2 that are essential for binding to SARS-CoV-2 spike are identical between humans and rhesus macaques (19). Therefore, we studied the pathogenesis of B.1.1.7 and B.1.351 in rhesus macaques and compared it to a recent SARS-CoV-2 isolate containing the D614G substitution in spike that rapidly became dominant globally in March 2020 (20) because of its increased transmissibility (21, 22). We found that B.1.351 was slightly less pathogenic than the other two variants, but there were no differences in virus shedding between the variants that could explain increased transmissibility.

RESULTS

Reduced disease in B.1.351-inoculated rhesus macaques

The pathogenicity of two VOC isolates, B.1.1.7 and B.1.351, was compared to the pathogenicity of a recent clade B.1 isolate containing the D614G substitution in the spike protein. First, we excluded that observed differences in our study were due to differences in binding of the spike protein of the different isolates to ACE2. We determined the binding efficiency of D614G, B.1.1.7, and B.1.351 spikes to human and rhesus macaque ACE2 using a vesicular stomatitis virus (VSV) pseudotype entry assay (23) and compared it to binding of the clade A prototype WA1 (nCOV-WA1-2020) spike. All the spike proteins

Copyright © 2021
The Authors, some
rights reserved;
exclusive licensee
American Association
for the Advancement
of Science. No claim to
original U.S. Government
Works. Distributed
under a Creative
Commons Attribution
License 4.0 (CC BY).

¹Laboratory of Virology, Division of Intramural Research, National Institute of Allergy and Infectious Diseases, National Institutes of Health, Hamilton, MT, USA. ²Rocky Mountain Veterinary Branch, Division of Intramural Research, National Institute of Allergy and Infectious Diseases, National Institutes of Health, Hamilton, MT, USA. ³Research Technologies Branch, Division of Intramural Research, National Institute of Allergy and Infectious Diseases, National Institutes of Health, Hamilton, MT, USA. *Corresponding author. Email: emmie.dewit@nih.gov

of the three isolates—D614G, B.1.1.7, and B.1.351—bound more efficiently to human and rhesus macaque ACE2 than the WA1 spike (fig. S1). However, there were no statistically significant differences in binding of the D614G versus the B.1.1.7 or B.1.351 spike to human or rhesus macaque ACE2 (fig. S1), indicating that any differences would not be caused by the efficiency of binding of spike to the ACE2 receptor. Three groups of six rhesus macaques were inoculated intranasally and intratracheally with a total dose of 2×10^6 median tissue culture infective dose (TCID₅₀) of one of the following SARS-CoV-2 isolates: SARS-CoV-2/human/USA/RML-7/2020, containing the D614G substitution in spike; hCoV_19/England/204820464/2020, a B.1.1.7 isolate; and hCoV-19/USA/MD-HP01542/2021, a B.1.351 isolate.

Clinical signs were mild in all three groups, with the main clinical signs observed being reduced appetite and changes in respiratory pattern (fig. S2). In addition, a clear nasal discharge was observed on 6 days post inoculation (dpi) in a single animal inoculated with D614G. Clinical scores were significantly lower in the animals inoculated with B.1.351 than B.1.1.7 and D614G on several days after inoculation (Fig. 1A). Further analysis of the clinical scores showed that this was due to a combination of differences in appetite and respiratory signs. The B.1.351-inoculated animals had fewer days with a reduced appetite, and only three of six animals inoculated with B.1.351 showed respiratory signs of disease at any time after inoculation compared with five of six for D614G and four of six for B.1.1.7 (fig. S2, A and B). No significant changes in bodyweight or body temperature were observed in any of the animals (fig. S2, C and D). Radiographs collected on 0, 2, 4, and 6 dpi were analyzed for the presence of pulmonary infiltrates. Pulmonary infiltrates were observed in most of the inoculated animals; however, no differences were observed between the three groups in the severity of infiltrates (Fig. 1B).

No difference in virus shedding between the three groups

Since increased virus shedding may lead to increased transmission efficiency, we studied virus shedding after inoculation as a proxy for transmission potential. Nose, throat, and rectal swabs were collected on 2, 4, and 6 dpi and analyzed for the presence of genomic RNA (gRNA), subgenomic RNA [sgRNA; an indicator of recent virus

replication (24)], and, in the case of nose and throat swab, infectious virus.

High amounts of gRNA, sgRNA, and high virus titers were observed in nose swabs (Fig. 2A) on 2 dpi, and these slowly declined over time. No differences in virus shedding from the nose were observed between the three groups. A similar pattern of virus shedding was observed in the throat swabs (Fig. 2B), again with no differences between the three groups. As previously observed (25–27), virus shedding was less consistent in the rectal swabs than in nose or throat swabs, but again, there were no differences between the three groups (Fig. 2C). In addition, gRNA nor sgRNA was detected in whole blood collected on 2, 4, and 6 dpi. To determine whether the total amount of virus shedding was different between the three groups, we also calculated the area under the curve for shedding of gRNA, sgRNA, and infectious virus in all swabs. No statistically significant differences in the total amount of shedding were detected (fig. S3A).

Similar virus replication kinetics in the airways during infection

As an indicator of virus replication in the lower respiratory tract during infection, bronchoalveolar lavage (BAL) and bronchial cytology brush (BCB) samples were collected on 2 and 4 dpi and analyzed for the presence of gRNA, sgRNA, and infectious virus. Viral loads and virus titer in BAL and BCB were highest on 2 dpi and declined by 4 dpi (fig. S3, B and C). Although viral loads and virus titers were generally higher in the BAL fluid than in the BCB sample, these two samples showed very similar kinetics overall, with samples with low viral loads in BAL also having low viral loads in BCB. No statistically significant differences were detected in viral RNA or virus titer in BAL or BCB between the three variants (fig. S3, B and C).

To determine whether single-nucleotide polymorphisms (SNPs) detected in the B.1.1.7 and B.1.351 virus stocks were stable in vivo, we performed next-generation sequencing of BAL samples collected on 2 dpi, close to the peak of virus replication. No SNPs were detected in the D614G inoculum at an allelic fraction >0.1, and only one SNP was detected in the BAL sample of one animal; this was a synonymous mutation in nsp6 (table S1). The B.1.1.7 inoculum contained

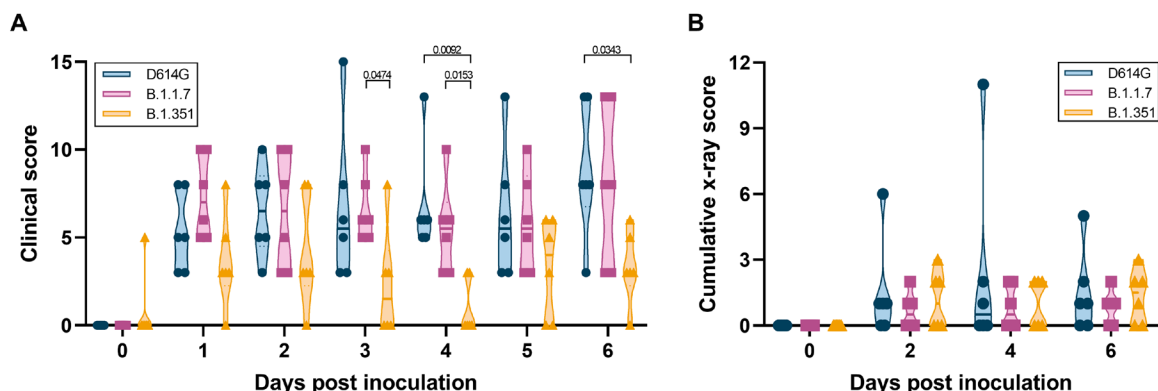


Fig. 1. Milder disease observed in rhesus macaques inoculated with B.1.351 than with D614G or B.1.1.7. Three groups of six adult rhesus macaques were inoculated with SARS-CoV-2 variants D614G, B.1.1.7, or B.1.351. After inoculation, animals were observed for disease signs and scored according to a preestablished clinical scoring sheet (A). Ventrodorsal and lateral radiographs were taken on clinical exam days and scored for the presence of pulmonary infiltrates by a clinical veterinarian according to a standard scoring system. Individual lobes were scored, and scores per animal per day were totaled and displayed (B). Center bars indicate the mean. Statistical analysis was performed using a two-way analysis of variance (ANOVA) with Tukey's multiple comparisons test; *P* values <0.05 are indicated.

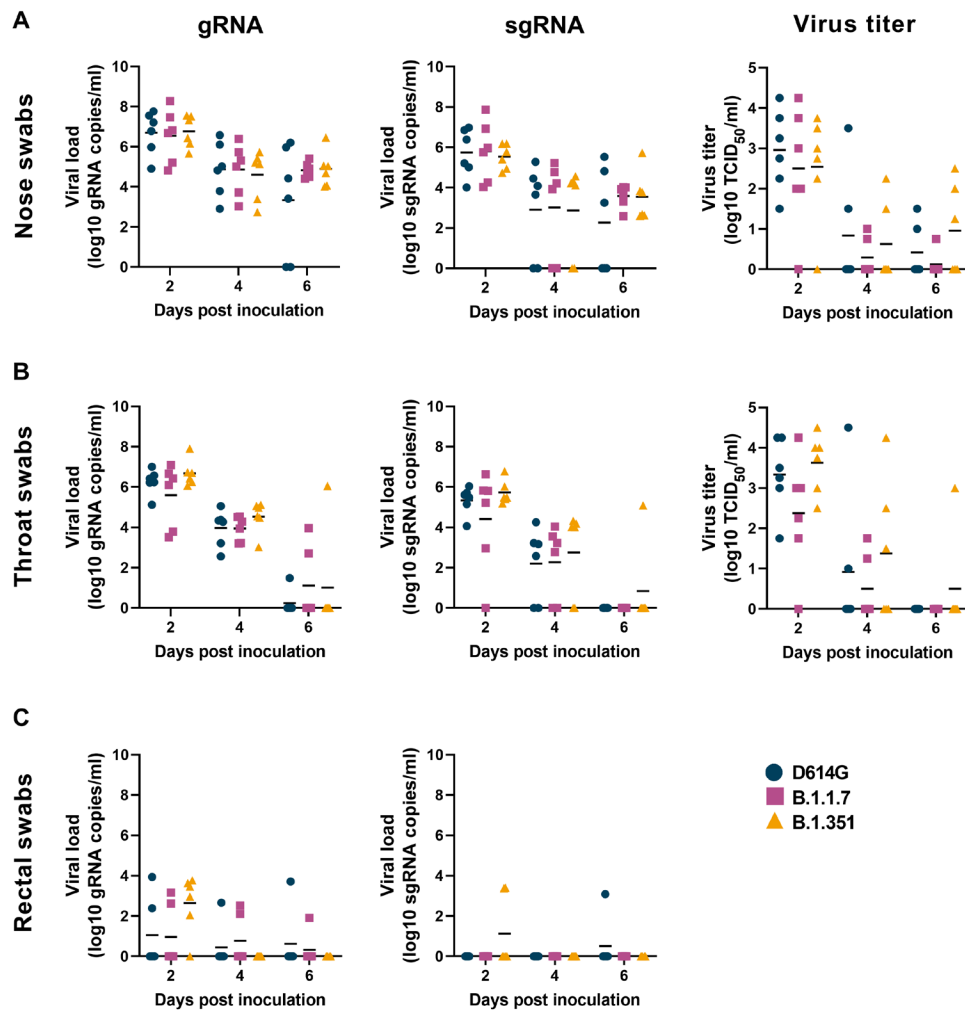


Fig. 2. No differences in virus shedding between D614G, B.1.1.7, and B.1.351. Three groups of six adult rhesus macaques were inoculated with SARS-CoV-2 variants D614G, B.1.1.7, or B.1.351. After inoculation, clinical exams were performed, during which nose (A), throat (B), and rectal (C) swabs were collected; viral loads and virus titers were measured in these samples. Quantitative reverse transcription polymerase chain reaction was performed to detect gRNA (left column) and sgRNA (middle column), and virus titration was performed on nose and throat swabs to detect levels of infectious virus (right column) in these samples. Lines indicate the mean. Statistical analysis was performed using a two-way ANOVA with Tukey's multiple comparisons test; no P values <0.05 were found.

three SNPs at >0.1 allelic fraction compared with the reference sequence; the D156G in nsp6 was detected in all animals, but at an allelic fraction <0.1 in five of six animals. The L257F substitution in nsp6 was maintained in all animals, and the V11I substitution increased in frequency in five of six animals (table S1). The B.1.351 inoculum contained two amino acid substitutions compared with the reference sequence; of these, the P252L substitution in nsp5 was maintained in five of six animals at slightly higher percentages than in the inoculum, whereas the L257F substitution in nsp6 was maintained at levels similar to the virus inoculum in all animals (table S1). Overall, the vast majority of amino acid substitutions present in the B.1.1.7 and B.1.351 inocula was maintained during replication in rhesus macaques, indicating that the effect of these substitutions on virus replication was most likely neutral in this host.

Lower virus titer in the lungs of B.1.351-inoculated animals

On 6 dpi, all animals were euthanized and necropsies were performed. To determine whether the presumed increased transmission of

B.1.1.7 or B.1.351 could be due to higher levels of virus replication in the nasal turbinates, we collected nasal turbinate material from three sites in the nasal turbinates and analyzed these for the presence of gRNA, sgRNA, and infectious virus (Fig. 3A). High viral loads of gRNA and sgRNA were detected in the nasal turbinates of all animals; fewer tissue samples were positive for sgRNA than gRNA, indicating that virus replication had peaked before the time of sampling. There were no statistically significant differences in viral loads between the variants (Fig. 3A). Fewer nasal turbinate samples had detectable infectious virus in the group of B.1.351-inoculated animals than in those inoculated with D614G or B.1.1.7, but this difference was not statistically significant (Fig. 3A). Similar analyses were performed on samples collected from all six lung lobes. Again, high viral loads of gRNA and sgRNA were detected, with fewer tissue samples being positive for sgRNA than gRNA (Fig. 3B). Significantly lower virus titers were detected in the lungs of B.1.351-inoculated animals than in those inoculated with D614G (Fig. 3B), possibly explaining the lower clinical scores observed in the animals inoculated with B.1.351 (Fig. 1A).

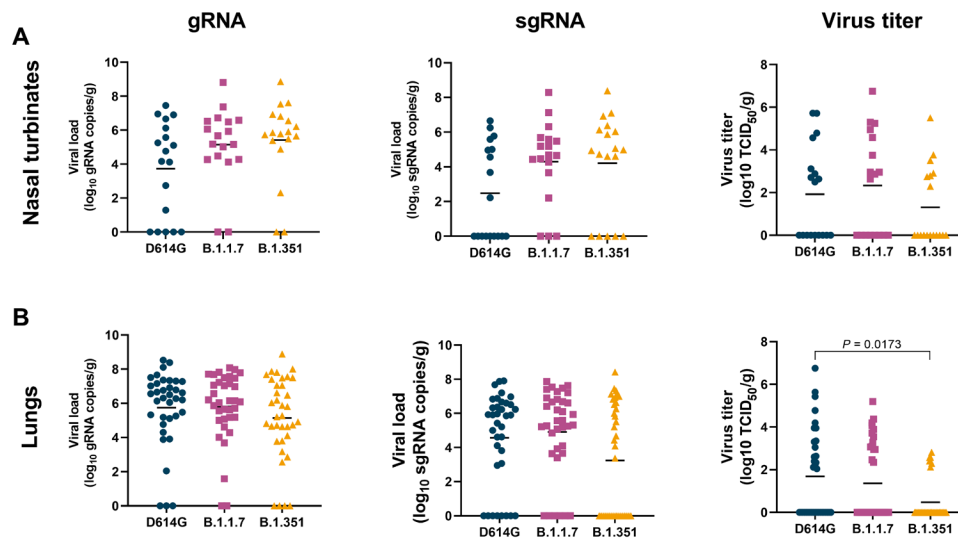


Fig. 3. Lower virus titers in lungs, but not nasal turbinates, of B.1.351-inoculated rhesus macaques. Three groups of six adult rhesus macaques were inoculated with SARS-CoV-2 variants D614G, B.1.1.7, or B.1.351. On 6 dpi, all animals were euthanized and necropsies were performed. Samples were collected from the frontal, mid, and rear nasal turbinates (A) as well as all six lung lobes (B) and analyzed for the presence of gRNA (left panels), sgRNA (middle panels), and virus titer (right panels). Lines indicate mean. Statistical analysis was performed using a Kruskal-Wallis test with Dunn's multiple comparisons tests, and P values <0.05 are indicated.

Additional tissue samples were analyzed for the presence of gRNA and sgRNA only. In the nasal mucosa, gRNA levels were significantly higher in B.1.1.7-inoculated animals than in the other two groups (fig. S4); however, this difference was not observed in sgRNA levels in the same tissues and thus probably does not represent increased virus replication in this tissue. Although B.1.1.7 appears to be detected in the various tissue samples more frequently than D614G and B.1.351, these differences were not statistically significant in individual tissues (fig. S4).

Less severe histologic lesions and viral antigen in the lungs of B.1.351-inoculated rhesus macaques

Lung tissues collected on 6 dpi were analyzed for the presence of histologic lesions. All inoculated animals developed some degree of pulmonary pathology, resulting in lesions typical of SARS-CoV-2 infection in rhesus macaques. On observation, lung lesions in animals inoculated with D614G were generally more severe than B.1.1.7 and B.1.351, while there were minimal differences between animals inoculated with B.1.1.7 and B.1.351 (Fig. 4, A to F). Analysis of the histology scores assigned to each lung lobe of all animals indicated that lesions in D614G-, B.1.1.7-, and B.1.351-inoculated animals occurred on a gradient from more to less severe, respectively; these differences were statistically significantly more severe in D614G- and B.1.1.7-inoculated animals than in B.1.351-inoculated animals (Fig. 4J). Immunohistochemistry was performed to detect SARS-CoV-2 antigen in lung tissue. As shown previously, viral antigen was present in type I and II pneumocytes, as well as alveolar macrophages. On observation, the animals inoculated with D614G generally had more viral antigen than those inoculated with B.1.1.7 or B.1.351 (Fig. 4, G to I). Analysis of the abundance of antigen presence in each lung lobe of all animals again indicated a gradient of viral antigen abundance from D614G to B.1.1.7 and B.1.351. There was statistically significantly more antigen present in the lungs of D614G-inoculated animals than in those inoculated with B.1.351 (Fig. 4K), in line with the lower virus titers detected in the lungs of these animals.

Viral antigen was also detected in the nasal epithelium of animals inoculated with all three isolates, but this was not associated with clear histologic lesions in any of the animals (fig. S5).

Subtle differences in local but not systemic innate immune response

We analyzed serum, BAL, and nasosorption samples for the presence of 10 cytokines and chemokines and found different responses in the different sample types. In serum, the immune response peaked at 2 dpi, with animals demonstrating up-regulation of interleukin-6 (IL-6), IL-15, IL-1 receptor antagonist (IL-1RA), monocyte chemoattractant protein-1 (MCP-1), interferon- α 2a (IFN- α 2a), and tumor necrosis factor- α (TNF- α), and was largely resolved by 4 dpi (Fig. 5A). Subtle differences between variant groups were observed in the levels of up-regulation of several cytokines, but the overall responses were largely similar (fig. S6A). Unsupervised hierarchical clustering confirmed this observation, with samples clustering by time point rather than variant group (Fig. 5A).

The cytokine and chemokine response in BAL was slightly delayed compared with that in serum, with the peak response at 4 dpi. This was defined by up-regulation of granulocyte-macrophage colony-stimulating factor (GM-CSF), MCP-1, and IL-15, indicating a concerted recruitment of leukocytes (Fig. 5B and fig. S4B). Notably, this response was absent in B.1.351-inoculated animals, as indicated by these samples clustering separately from D614G- and B.1.1.7-inoculated animals (Fig. 5B). The limited immune response in the BAL of B.1.351-inoculated animals is in agreement with the reduced lung virus titers and histologic lesion severity observed in these animals (Figs. 3B and 4, I to J), suggesting reduced pathogenicity in the lower respiratory tract.

In nasal samples, we observed a notable difference in the immune response in B.1.1.7-inoculated animals compared with those inoculated with D614G and B.1.351. Samples from B.1.1.7-inoculated animals at all time points clustered separately and showed a unique proinflammatory response consisting of up-regulation of IL-6, MCP-1,

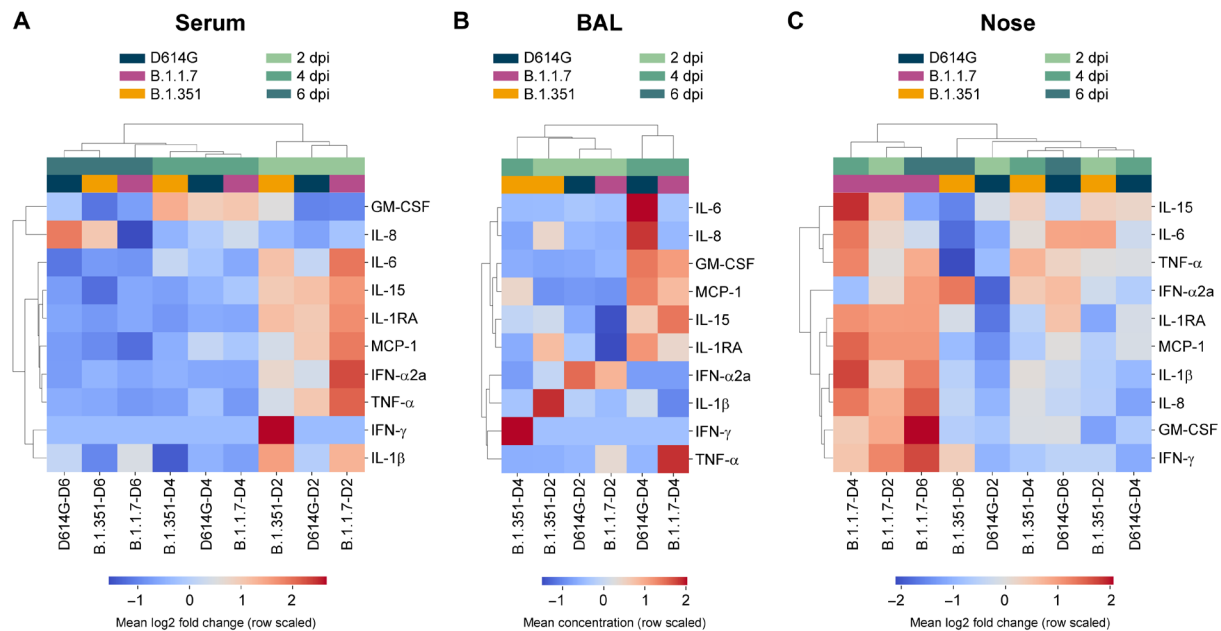


Fig. 5. Differences in cytokine and chemokine levels in serum, BAL, and nose samples of rhesus macaques inoculated with D614G, B.1.1.7, or B.1.351. Three groups of six adult rhesus macaques were inoculated with SARS-CoV-2 variants D614G, B.1.1.7, or B.1.351. The levels of 10 cytokines and chemokines were determined in serum on 0, 2, 4, and 6 dpi (A); in BAL on 2 and 4 dpi (B); and in nasal samples on 0, 2, 4, and 6 dpi (C). For serum and nasal samples, fold change in cytokine/chemokine level is shown normalized to baseline levels measured on 0 dpi. For BAL samples, concentrations are shown. Data represent the mean log₂ fold change or concentration of analytes in variant groups at each time point and are organized according to unsupervised hierarchical clustering.

individuals does not necessarily mean an overall decrease in virulence, since increased transmission of these variants could result in an increased disease burden of these variants on the population level (28).

The reduced replication of B.1.351 in the lower, but not upper, respiratory tract might imply that this virus is evolving to become more like a virus of the upper respiratory tract. Likewise, the only difference observed in our study between B.1.1.7 and D614G was in the innate immune response in the upper, but not lower, respiratory tract.

The virus shedding data in swabs collected from the upper respiratory tract did not directly explain the increased transmission of B.1.1.7 and B.1.351 observed in the population. However, the up-regulation of innate immune responses in the nasal samples collected from B.1.1.7-inoculated animals may potentially play a role in the increased transmission of this variant. Nasal inflammatory responses such as the increased cytokine and chemokine concentrations observed here have been linked to common cold symptoms in humans (29, 30). Symptomatic 229E coronavirus infection in human volunteers was linked to increased plasma exudation into the nasal cavity (31). One potential explanation for increased transmission of B.1.1.7 could be that increased protein concentrations in nasal secretions caused by plasma exudation could stabilize the virus in respiratory droplets (32). Alternatively, symptomatic 229E infection leads to an increase in nasal mucosal temperature (31), which may affect the viscosity of nasal secretions and thereby the production of respiratory droplets.

One limitation of our study is the lack of comorbidities and severe disease manifestations in the rhesus macaque model. However, the age range of the animals used in this study (age range, 2 to 16 years) is probably a fair reflection of the population currently exhibiting

the highest prevalence of SARS-CoV-2 infections, which appears to be younger than early during the COVID-19 pandemic (33). Despite the lower pathogenicity of B.1.351 overall, severe disease is still expected to occur in individuals with comorbidities. More targeted epidemiological studies are needed to clarify the impact of VOC on the disease burden in various subpopulations with and without comorbidities while excluding the effect of confounding factors such as the overall number of cases and changes in human behavior.

The B.1.351 lineage has been associated with reduced neutralization by convalescent sera of humans previously infected with SARS-CoV-2 and in people vaccinated against SARS-CoV-2 (34). In addition, reduced vaccine efficacy against mild-to-moderate COVID-19 was observed with the B.1.351 variant for vaccines tested in multicenter clinical trials in South Africa and Qatar (35, 36). Rechallenge studies in hamsters suggest that prior exposure to SARS-CoV-2 protects against disease but not reinfection of the upper respiratory tract (37). These studies, together with our side-by-side comparison of three SARS-CoV-2 variants in the most relevant animal model for pre-clinical development and comparative pathogenicity, suggest that ongoing circulation under diverse evolutionary pressures favors transmissibility and immune evasion rather than an increase in intrinsic pathogenicity.

MATERIALS AND METHODS

Study design

To compare the pathogenicity and virus shedding of VOC B.1.1.7 and B.1.351, we inoculated three groups of six rhesus macaques with three different SARS-CoV-2 isolates: SARS-CoV-2/human/USA/RML-7/2020, a contemporary clade B.1 isolate containing the D614G substitution in spike; hCoV_19/England/204820464/2020,

a B.1.1.7 isolate; and hCoV-19/USA/MD-HP01542/2021, a B.1.351 isolate. Each group of six animals contained one older adult animal (age 15 to 16 years), one adult animal (age 3 to 5 years), and four young rhesus macaques (age 2 to 3 years); ages of individual animals are listed in table S2. All but one of the older animals were male. Each group of animals was housed in a separate room. The animals were inoculated intranasally via a MAD Nasal IN Mucosal Atomization device (0.5 ml per nostril; Teleflex, USA) and intratracheally (4 ml) with an inoculum of 4×10^5 TCID₅₀/ml virus dilution in sterile Dulbecco's modified Eagle's medium (DMEM), resulting in a total dose of 2×10^6 TCID₅₀. The intranasal administration using an atomization device was done as a refinement to improve distribution of the inoculum throughout the nasal cavity, since replication in the upper respiratory tract could be an important factor to explain the observed increased transmission of the VOC. The inocula were titered on Vero E6 cells to confirm that the correct dose was administered. The animals were observed and scored daily according to a standardized scoring sheet (26); the same person, blinded to the isolate that the animals received, assessed the animals throughout the study. The predetermined end point for this experiment was 6 dpi. Clinical exams were performed on 0, 2, 4, and 6 dpi on anesthetized animals. On exam days, clinical parameters such as body weight, body temperature, and respiratory rate were collected. In addition, ventrodorsal and right/left lateral thoracic radiographs were taken before any other procedures (e.g., BAL and nasal flush). Radiographs were evaluated and scored for the presence of pulmonary infiltrates by two board-certified clinical veterinarians according to a standard scoring system. Briefly, each lung lobe (upper left, middle left, lower left, upper right, middle right, and lower right) was scored individually on the basis of the following criteria: 0 = normal examination; 1 = mild interstitial pulmonary infiltrates; 2 = moderate interstitial pulmonary infiltrates, perhaps with partial cardiac border effacement and small areas of pulmonary consolidation (alveolar patterns and air bronchograms); and 3 = pulmonary consolidation as the primary lung pathology, seen as a progression from grade 2 lung pathology. At study completion, thoracic radiograph findings are reported as a single radiograph score for each animal on each exam day. To obtain this score, the scores assigned to each of the six lung lobes are added together and recorded as the radiograph score for each animal on each exam day. Scores may range from 0 to 18 for each animal on each exam day. Blood as well as nasal, throat, and rectal swabs were collected during all clinical exams. Nasosorption swabs were collected from the nostril that was not used for nasal swabbing; nasosorption swabs were inserted in the nostril and kept in place for 1 min. Nasosorption swabs were collected in 300 μ l of PBS containing 1% bovine serum albumin and 0.4% Tween 20 and vortexed for 30 s. The swab and liquid were then placed on a spin filter (Agilent, 5185-5990) and centrifuged at 16,000 rpm for 20 min. Filtered liquid was aliquoted and stored at -80°C . In addition, on 2 and 4 dpi, animals were intubated and BALs were performed using 10 ml of sterile saline, and a second sample was collected in the same location using a cytology brush (BCB). The brush was then placed in 1 ml of DMEM containing penicillin (50 U/ml) and streptomycin (50 μ g/ml). On 6 dpi, all animals were euthanized; after euthanasia, necropsies were performed, and tissue samples were collected. Histopathological analysis of tissue slides was performed by a board-certified veterinary pathologist blinded to the group assignment of the animals.

Ethics and biosafety statement

All animal experiments were approved by the Institutional Animal Care and Use Committee of Rocky Mountain Laboratories, National Institutes of Health (NIH), and carried out in an Association for Assessment and Accreditation of Laboratory Animal Care (AAALAC) International-accredited facility, according to the institution's guidelines for animal use, following the guidelines and basic principles in the NIH *Guide for the Care and Use of Laboratory Animals*, the Animal Welfare Act, U.S. Department of Agriculture, and the U.S. Public Health Service Policy on Humane Care and Use of Laboratory Animals. Rhesus macaques were housed in adjacent individual primate cages, allowing social interactions, within a climate-controlled room with a fixed light-dark cycle (12-hour light/12-hour dark). Animals were monitored at least twice daily throughout the experiment. Commercial monkey chow was provided twice daily, and the diet was supplemented with treats, vegetables, and/or fruit at least once a day. Water was available ad libitum. Environmental enrichment consisted of a variety of human interaction, manipulanda, commercial toys, videos, and music. The Institutional Biosafety Committee (IBC) approved work with infectious SARS-CoV-2 strains under Biosafety Level 3 conditions. Sample inactivation was performed according to IBC-approved standard operating procedures for removal of specimens from high containment.

Virus and cells

SARS-CoV-2/human/USA/RML-7/2020 (GenBank: MW127503.1; designated D614G throughout the manuscript) was obtained from a nasopharyngeal swab obtained on 19 July 2020. Two passages of the original swab were performed in Vero E6 cells. The virus stock used was 100% identical to the deposited GenBank sequence. hCoV-19/England/204820464/2020 (GISAID: EPI_ISL_683466; designated B.1.1.7 throughout the manuscript) was obtained from Public Health Agency England via BEI Resources. The obtained passage 2 material was propagated once in Vero E6 cells. Sequencing confirmed the presence of the following three SNPs in this stock: nsp6 D156G (present in 14% of all reads), nsp6 L257F (18%), and nsp7 V11I (13%). hCoV-19/USA/MD-HP01542/2021 (GISAID: EPI_ISL_890360; designated B.1.351 throughout the manuscript) was obtained from A. Pekosz at the Johns Hopkins University Bloomberg School of Public Health. The obtained passage 2 material was propagated once in Vero E6 cells. Sequencing confirmed the presence of two SNPs in this stock: nsp5 P252L (17%) and nsp6 L257F (57%). The D614G, B.1.1.7, and B.1.351 stocks contained similar ratios of SARS-CoV-2 E gene copies to infectious virus, i.e., 1.3×10^4 , 1.6×10^4 , and 1.5×10^4 RNA copies/TCID₅₀, respectively.

Vero E6 cells were maintained in DMEM supplemented with 10% fetal bovine serum (FBS), 1 mM L-glutamine, penicillin (50 U/ml), and streptomycin (50 μ g/ml); SARS-CoV-2 stocks were grown in the same medium, except with 2% FBS.

Pseudotype virus entry assay

Assays were performed as described previously (23). Briefly, the spike coding sequences of SARS-CoV-2 variants were truncated by deleting 19 amino acids at the C terminus to increase efficient incorporation into virions of VSV (38, 39), codon optimized for human cells, and appended with a 5' kozak expression sequence (GCCACC) and 3' tetraglycine linker followed by nucleotides encoding a FLAG-tag sequence (DYKDDDDK). All spikes, human and rhesus macaque ACE2 sequences (Q9BYF1.2 and FJ170099.1, respectively), were

synthesized, cloned into pcDNA3.1+ (GenScript), and verified by Sanger sequencing.

For pseudotype production, plates precoated with poly-L-lysine (Sigma-Aldrich) were seeded with 293T cells and transfected the following day with 1200 ng of empty plasmid and 400 ng of plasmid encoding coronavirus spike or no-spike plasmid control [green fluorescent protein (GFP)]. After 24 hours, transfected cells were infected with VSVΔG seed particles pseudotyped with VSV-G. After 1 hour of incubating with intermittent shaking at 37°C, cells were washed four times and incubated in 2 ml of DMEM supplemented with 2% FBS, penicillin/streptomycin, and L-glutamine for 48 hours. Supernatants were collected, centrifuged at 500g for 5 min, aliquoted, and stored at –80°C.

Baby hamster kidney cells were seeded in black 96-well plates and transfected the next day with 100 ng of plasmid DNA encoding human or rhesus macaque ACE2 using polyethylenimine (Polysciences). Twenty-four hours after transfection, cells were inoculated with equivalent volumes of pseudotype stocks, in octuplet. Plates were then centrifuged at 1200g at 4°C for 1 hour and incubated overnight at 37°C. Approximately 18 to 20 hours after infection, Bright-Glo luciferase reagent (Promega) was added to each well (1:1), and luciferase was measured. Relative entry was calculated normalizing the relative light unit for spike pseudotypes to the plate relative light unit average for the no-spike control.

Quantitative polymerase chain reaction

RNA was extracted from swabs and BAL using the QiaAmp Viral RNA Kit (QIAGEN) according to the manufacturer's instructions. Tissues (30 mg) were homogenized in RLT buffer, and RNA was extracted using the RNeasy Kit (QIAGEN) according to the manufacturer's instructions. For detection of gRNA (E) and sgRNA (E), 5 μl of RNA was used in a one-step real-time reverse transcription polymerase chain reaction (RT-PCR) assay (40, 41) using the QuantiFast Probe Kit (QIAGEN) according to the manufacturer's instructions. In each run, standard dilutions of counted RNA standards were run in parallel to calculate the copy numbers in the samples.

Virus titration

Virus titrations were performed by end-point titration in Vero E6 cells. Tissues were homogenized in 1 ml of DMEM using a TissueLyser II (QIAGEN) and a 5-mm stainless steel bead. Cells were inoculated with 10-fold serial dilutions of swab, BAL, BCB, or homogenized tissue samples in 96-well plates. Plates were centrifuged for 30 min at 1000 rpm and incubated for 30 min at 37°C and 5% CO₂. The inoculum was then removed and replaced with 100 μl of DMEM containing 2% FBS, penicillin (50 U/ml), and streptomycin (50 μg/ml). Six days after inoculation, the cytopathic effect (CPE) was scored and the TCID₅₀ was calculated.

Next-generation sequencing of viral RNA

Viral RNA was extracted as described above. KAPA's RNA Hyper-Prep library preparation kit (Roche Sequencing Solutions) was used to prepare sequencing libraries 10 μl RNA. To facilitate multiplexing, adapter ligation was performed with the KAPA Universal Adapter and Unique Dual-Indexed Primer mixes. Samples were enriched for adapter-ligated product using KAPA HiFi HotStart Ready mix and 12 PCR amplification cycles according to the manufacturer's manual. Pools consisting of 8 to 10 sample libraries were used for hybrid-capture virus enrichment using myBaits Expert Virus SARS-CoV-2

panel and following the manufacturer's manual, version 4.01, with 8 to 13 cycles of postcapture PCR amplification (Arbor Biosciences). Purified, enriched libraries were quantified using a KAPA Library Quantification kit (Roche Sequencing Solutions) and sequenced as 2 × 150-base pair reads on the Illumina NextSeq 550 instrument (Illumina).

Raw fastq reads were trimmed of Illumina adapter sequences using cutadapt version 1.12 (42) and then trimmed and filtered for quality using the FASTX-Toolkit (Hannon Lab). Remaining reads were mapped to the respective hCoV_19/England/204820464/2020, hCoV-19/USA/MD-HP01542/2021, and SARS-CoV-2/human/USA/RML-7/2020 genomes using Bowtie2 version 2.2.9 with parameters `--local --no-mixed -X 1500`. PCR duplicates were removed using picard MarkDuplicates (Broad Institute), and variants were called using GATK Haplotype-Caller version 4.1.2.0 (43) with parameter `-ploidy 2`. Variants were filtered for `QUAL > 500` and `DP > 20` using BCFtools.

Histopathology

Histopathology and immunohistochemistry were performed on rhesus macaque tissues. After fixation for a minimum of 7 days in 10% neutral-buffered formalin and embedding in paraffin, tissue sections were stained with hematoxylin and eosin. Immunohistochemistry was performed using a custom-made rabbit antiserum against SARS-CoV-2 N at a 1:1000 dilution. Stained slides were analyzed by a board-certified veterinary pathologist. Histologic lesion severity was scored per lung lobe according to a standardized scoring system evaluating the presence of interstitial pneumonia, type II pneumocyte hyperplasia, edema and fibrin, and perivascular lymphoid cuffing: 0, no lesions; 1, minimal (1 to 10% of lobe affected); 2, mild (11 to 25%); 3, moderate (26 to 50%); 4, marked (51 to 75%); and 5, severe (76 to 100%). Presence of viral antigen was scored per lung lobe according to a standardized scoring system: 0, none; 1, rare/few; 2, scattered; 3, moderate; 4, numerous; and 5, diffuse.

Cytokine and chemokine analysis

Serum, BAL fluid, and nasosorption samples were analyzed for the presence of GM-CSF, MCP-1, TNF-α, IFN-α2a, IFN-γ, IL-1RA, IL-1β, IL-6, IL-8, and IL-15 using the U-PLEX NHP Biomarker Group 1 Kit (Meso Scale Diagnostics) according to the manufacturer's instructions. Plates were read using a MESO QuickPlex SQ 120 instrument (Meso Scale Diagnostics). Samples from animals inoculated with different variants were randomized across plates to mitigate batch effects. Samples were inactivated via 2MRad gamma-irradiation before analysis outside of containment (44). For BAL samples, 0.1% Triton X-100 (Sigma-Aldrich) was added immediately before running the assay to prevent clumping. Analyte concentrations and upper and lower detection limits were determined using the Discovery Workbench software (Meso Scale Diagnostics) individually for each assay plate. Samples that fell below the lower detection limit were replaced with the corresponding lower detection limit value. Data were analyzed using Python (version 3.8.5) and GraphPad Prism (version 8.2.1). To correct for baseline differences in cytokine concentrations between animals, the log₂ fold change of analytes was calculated on a per-animal basis using the 0-dpi sample as a baseline. Log₂ fold changes were not calculated for BAL samples, as a 0-dpi sample was not available. Unsupervised hierarchical clustering (Ward's) was performed on Euclidean pairwise distance matrices calculated from the mean of the log₂ fold change or concentration of analytes from animals in each group at each available time point

using SciPy (version 1.6.0) and Seaborn (version 0.11.1) packages in Python.

Statistical analysis

Statistical analyses were performed using GraphPad Prism software version 8.2.1. Correlation analysis was performed in Python (version 3.8.5) using the pairwise_corr function from the package pingouin (version 0.3.10) with options method = spearman and padjust = sidak. For all analyses, a *P* value of 0.05 was used as cutoff for statistical significance.

SUPPLEMENTARY MATERIALS

Supplementary material for this article is available at <https://science.org/doi/10.1126/sciadv.abj3627>

[View/request a protocol for this paper from Bio-protocol.](#)

REFERENCES AND NOTES

- World Health Organization, *COVID-19 Weekly Epidemiological Update* (World Health Organization, 2021); www.who.int/docs/default-source/coronaviruse/situation-reports/20210225_weekly_epi_update_voc-special-edition.pdf.
- N. G. Davies, S. Abbott, R. C. Barnard, C. I. Jarvis, A. J. Kucharski, J. D. Munday, C. A. B. Pearson, T. W. Russell, D. C. Tully, A. D. Washburne, T. Wenseleers, A. Gimma, W. Waites, K. L. M. Wong, K. van Zandvoort, J. D. Silverman; CMMID COVID-Working Group; COVID-19 Genomics UK (COG-UK) Consortium, K. Diaz-Ordaz, R. Keogh, R. M. Eggo, S. Funk, M. Jit, K. E. Atkins, W. J. Edmunds, Estimated transmissibility and impact of SARS-CoV-2 lineage B.1.1.7 in England. *Science* **372**, eabg3055 (2021).
- E. Volz, S. Mishra, M. Chand, J. C. Barrett, R. Johnson, L. Geidelberg, W. R. Hinsley, D. J. Laydon, G. Dabrera, A. O'Toole, R. Amato, M. Ragonnet-Cronin, I. Harrison, B. Jackson, C. V. Ariani, O. Boyd, N. J. Loman, J. T. Mc Crone, S. Gonçalves, D. Jorgensen, R. Myers, V. Hill, D. K. Jackson, K. Gaythorpe, N. Groves, J. Sillitoe, D. P. Kwiatkowski; The COVID-19 Genomics UK (COG-UK) consortium, S. Flaxman, O. Ratmann, S. Bhatt, S. Hopkins, A. Gandy, A. Rambaut, N. M. Ferguson, Assessing transmissibility of SARS-CoV-2 lineage B.1.1.7 in England. *Nature* **593**, 266–269 (2021).
- M. S. Graham, C. H. Sudre, A. May, M. Antonelli, B. Murray, T. Varsavsky, K. Kläser, L. S. Canas, E. Molteni, M. Modat, D. A. Drew, L. H. Nguyen, L. Polidori, S. Selvaichandran, C. Hu, J. Capdevila; COVID-19 Genomics UK (COG-UK) Consortium, A. Hammers, A. T. Chan, J. Wolf, T. D. Spector, C. J. Steves, S. Ourselin, Changes in symptomatology, reinfection, and transmissibility associated with the SARS-CoV-2 variant B.1.1.7: An ecological study. *Lancet Public Health* **6**, e335–e345 (2021).
- N. L. Washington, K. Gangavarapu, M. Zeller, A. Bolze, E. T. Cirulli, K. M. S. Barrett, B. B. Larsen, C. Anderson, S. White, T. Cassens, S. Jacobs, G. Levan, J. Nguyen, J. M. Ramirez III, C. Rivera-Garcia, E. Sandoval, X. Wang, D. Wong, E. Spencer, R. Robles-Sikisaka, E. Kurzban, L. D. Hughes, X. Deng, C. Wang, V. Servellita, H. Valentine, P. De Hoff, P. Seaver, S. Sathe, K. Gietzen, B. Sickler, J. Antico, K. Hoon, J. Liu, A. Harding, O. Bakhtar, T. Basler, B. Austin, D. M. Cannell, M. Isaksson, P. G. Febbo, D. Becker, M. Laurent, E. M. Donald, G. W. Yeo, R. Knight, L. C. Laurent, E. de Feo, M. Worobey, C. Y. Chiu, M. A. Suchard, J. T. Lu, W. Lee, K. G. Anderson, Emergence and rapid transmission of SARS-CoV-2 B.1.1.7 in the United States. *Cell* **184**, 2587–2594.e7 (2021).
- L. Y. W. Lee, S. Rozmanowski, M. Pang, A. Charlett, C. Anderson, G. J. Hughes, M. Barnard, L. Peto, R. Vipond, A. Sienkiewicz, S. Hopkins, J. Bell, D. W. Crook, N. Gent, A. S. Walker, T. E. A. Peto, D. W. Eyre, SARS-CoV-2 infectivity by viral load, S gene variants and demographic factors and the utility of lateral flow devices to prevent transmission. *Clin. Infect. Dis.*, ciab421 (2021).
- S. M. Kissler, J. R. Fauver, C. Mack, C. G. Tai, M. I. Breban, A. E. Watkins, R. M. Samant, D. J. Anderson, D. D. Ho, N. D. Grubaugh, Y. H. Grad, Densely sampled viral trajectories suggest longer duration of acute infection with B.1.1.7 variant relative to non-B.1.1.7 SARS-CoV-2. *medRxiv*, 2021.02.16.21251535 (2021). <https://doi.org/10.1101/2021.02.16.21251535>.
- N. G. Davies, C. I. Jarvis; CMMID COVID-19 Working Group, W. John Edmunds, N. P. Jewell, K. Diaz-Ordaz, R. H. Keogh, Increased mortality in community-tested cases of SARS-CoV-2 lineage B.1.1.7. *Nature* **593**, 270–274 (2021).
- D. Frampton, T. Rampling, A. Cross, H. Bailey, J. Heaney, J. Heaney, R. Scott, R. Sconza, J. Price, M. Margaritis, M. Bergstrom, M. J. Spyer, P. B. Miralhes, P. Grant, S. Kirk, C. Valerio, Z. Mangera, T. Prabhakar, J. Moreno-Cuesta, N. Arulkumaran, M. Singer, G. Y. Shin, E. Sanchez, S. M. Paraskevopoulou, D. Pillay, R. A. McKendry, M. Mirfenderesky, C. F. Houlihan, E. Nastouli, Genomic characteristics and clinical effect of the emergent SARS-CoV-2 B.1.1.7 lineage in London, UK: A whole-genome sequencing and hospital-based cohort study. *Lancet Infect. Dis.* **21**, 1246–1256 (2021).
- R. Challen, E. Brooks-Pollock, J. M. Read, L. Dyson, K. Tsaneva-Atanasova, L. Danon, Risk of mortality in patients infected with SARS-CoV-2 variant of concern 202012/1: Matched cohort study. *BMJ* **372**, n579 (2021).
- L. B. Snell, W. Wang, A. Alcolea-Medina, T. Charalampous, G. Nebbia, R. Batra, L. de Jongh, F. Higgins, Y. Wang, J. D. Edgeworth, V. Curcin, First and second SARS-CoV-2 waves in inner London: A comparison of admission characteristics and the impact of the B.1.1.7 variant. *medRxiv* 2021.03.16.21253377 (2021); <https://doi.org/10.1101/2021.03.16.21253377>.
- H. Tegally, E. Wilkinson, M. Giovanetti, A. Iranzadeh, V. Fonseca, J. Giandhari, D. Doolabh, S. Pillay, E. J. San, N. Msomi, K. Misana, A. von Gottberg, S. Walaza, M. Allam, A. Ismail, T. Mohale, A. J. Glass, S. Engelbrecht, G. van Zyl, W. Preiser, F. Petruccione, A. Sigal, D. Hardie, G. Marais, N.-y. Hsiao, S. Korsman, M.-A. Davies, L. Tyers, I. Mudau, D. York, C. Maslo, D. Goedhals, S. Abrahams, O. Laguda-Akingba, A. Alisoltani-Dehkordi, A. Godzik, C. K. Wibmer, B. T. Sewell, J. Lourenço, L. C. J. Alcántara, S. L. Kosakovsky Pond, S. Weaver, D. Martin, R. J. Lessells, J. N. Bhiman, C. Williamson, T. de Oliveira, Detection of a SARS-CoV-2 variant of concern in South Africa. *Nature* **592**, 438–443 (2021).
- W. Jassat, C. Mudara, L. Ozougwu, S. Tempia, L. Blumberg, M.-A. Davies, Y. Pillay, T. Carter, R. Morewane, M. Wolmarans, A. von Gottberg, J. N. Bhiman, S. Walaza; DATCOV Author Group, C. Cohen, Increased mortality among individuals hospitalized with COVID-19 during the second wave in South Africa. *medRxiv* 2021.03.09.21253184 (2021); <https://doi.org/10.1101/2021.03.09.21253184>.
- C. A. B. Pearson, T. W. Russell, N. Davies, A. J. Kucharski; CMMID COVID-19 working group, W. John Edmunds, R. M. Eggo, Estimates of severity and transmissibility of novel SARS-CoV-2 variant 501Y.V2 in South Africa (CMMID, 2021); <https://cmmid.github.io/topics/covid19/sa-novel-variant.html>.
- I. A. Nuñez, C. Z. Lien, P. Selvaraj, C. B. Stauff, S. Liu, M. F. Starost, T. T. Wang, SARS-CoV-2 B.1.1.7 infection of Syrian hamster does not cause more severe disease and is protected by naturally acquired immunity. *mSphere* **6**, e00507–e00521 (2021).
- S. Mohandas, P. D. Yadav, D. Nyayanit, G. Deshpande, A. Shete-Aich, G. Sapkal, S. Kumar, R. Jain, M. Kadam, A. Kumar, D. Y. Patil, P. D. Sarkale, P. Gawande, P. Abraham, Comparison of the pathogenicity and virus shedding of SARS-CoV-2 VOC 202012/01 and D614G variant in hamster model. *BioRxiv* 2021.02.25.432136 (2021); <https://doi.org/10.1101/2021.02.25.432136>.
- R. Abdelnabi, R. Boudewijns, C. S. Foo, L. Seldeslachts, L. Sanchez-Felipe, X. Zhang, L. Delang, P. Maes, S. J. F. Kaptein, B. Weynand, G. Vande Velde, J. Neyts, K. Dallmeier, Comparing infectivity and virulence of emerging SARS-CoV-2 variants in Syrian hamsters. *EBioMedicine* **68**, 103403 (2021).
- C. Munoz-Fontela, W. E. Dowling, S. G. P. Funnell, P.-S. Gsell, A. Ximena Riveros-Balta, R. A. Albrecht, H. Andersen, R. S. Baric, M. W. Carroll, M. Cavaleri, C. Qin, I. Crozier, K. Dallmeier, L. de Waal, E. de Wit, L. Delang, E. Dohm, W. P. Duprex, D. Falzarano, C. L. Finch, M. B. Frieman, B. S. Graham, L. E. Gralinski, K. Guilfoyle, B. L. Haagmans, G. A. Hamilton, A. L. Hartman, S. Herfst, S. J. F. Kaptein, W. B. Klimstra, I. Knezevic, P. R. Krause, J. H. Kuhn, R. L. Grand, M. G. Lewis, W.-C. Liu, P. Maisonnasse, A. K. Mc Elroy, V. Munster, N. Oreshkova, A. L. Rasmussen, J. Rocha-Pereira, B. Rockx, E. Rodriguez, T. F. Rogers, F. J. Salguero, M. Schotsaert, K. J. Stittelaar, H. J. Thibaut, C.-T. Tseng, J. Vergara-Alert, M. Beer, T. Brasel, J. F. W. Chan, A. Garcia-Sastre, J. Neyts, S. Perlman, D. S. Reed, J. A. Richt, C. J. Roy, J. Segalés, S. S. Vasan, A. M. Henao-Restrepo, D. H. Barouch, Animal models for COVID-19. *Nature* **586**, 509–515 (2020).
- A. D. Melin, M. C. Janiak, F. Marrone III, P. S. Arora, J. P. Higham, Comparative ACE2 variation and primate COVID-19 risk. *Commun. Biol.* **3**, 641 (2020).
- B. Korber, W. M. Fischer, S. Gnanakaran, H. Yoon, J. Theiler, W. Abfalterer, N. Hengartner, E. E. Giorgi, T. Bhattacharya, B. Foley, K. M. Hastie, M. D. Parker, D. G. Partridge, C. M. Evans, T. M. Freeman, T. I. de Silva, Tracking changes in SARS-CoV-2 spike: Evidence that D614G increases infectivity of the COVID-19 virus. *Cell* **182**, 812–827.e19 (2020).
- Y. J. Hou, S. Chiba, P. Halfmann, C. Ehre, M. Kuroda, K. H. Dinnon III, S. R. Leist, A. Schäfer, N. Nakajima, K. Takahashi, R. E. Lee, T. M. Mascenik, R. Graham, C. E. Edwards, L. V. Tse, K. Okuda, A. J. Markmann, L. Bartelt, A. de Silva, D. M. Margolis, R. C. Boucher, S. H. Randell, T. Suzuki, L. E. Gralinski, Y. Kawaoka, R. S. Baric, SARS-CoV-2 D614G variant exhibits efficient replication ex vivo and transmission in vivo. *Science* **370**, 1464–1468 (2020).
- J. A. Plante, Y. Liu, J. Liu, H. Xia, B. A. Johnson, K. G. Lokugamage, X. Zhang, A. E. Muruato, J. Zou, C. R. Fontes-Garfias, D. Mirchandani, D. Scharton, J. P. Bilello, Z. Ku, Z. An, B. Kalveram, A. N. Freiberg, V. D. Menachery, X. Xie, K. S. Plante, S. C. Weaver, P. Y. Shi, Spike mutation D614G alters SARS-CoV-2 fitness. *Nature* **592**, 116–121 (2021).
- M. Letko, A. Marzi, V. Munster, Functional assessment of cell entry and receptor usage for SARS-CoV-2 and other lineage B betacoronaviruses. *Nat. Microbiol.* **5**, 562–569 (2020).
- E. Speranza, B. N. Williamson, F. Feldmann, G. L. Sturdevant, L. Pérez-Pérez, K. Meade-White, B. J. Smith, J. Lovaglio, C. Martens, V. J. Munster, A. Okumura, C. Shaia, H. Feldmann, S. M. Best, E. de Wit, Single-cell RNA sequencing reveals SARS-CoV-2 infection dynamics in lungs of African green monkeys. *Sci. Transl. Med.* **13**, eabe8146 (2021).
- W. Deng, L. Bao, J. Liu, C. Xiao, J. Liu, J. Xue, Q. Lv, F. Qi, H. Gao, P. Yu, Y. Xu, Y. Qu, F. Li, Z. Xiang, H. Yu, S. Gong, M. Liu, G. Wang, S. Wang, Z. Song, Y. Liu, W. Zhao, Y. Han, L. Zhao,

- X. Liu, Q. Wei, C. Qin, Primary exposure to SARS-CoV-2 protects against reinfection in rhesus macaques. *Science* **369**, 818–823 (2020).
26. V. J. Munster, F. Feldmann, B. N. Williamson, N. van Doremalen, L. Pérez-Pérez, J. Schulz, K. Meade-White, A. Okumura, J. Callison, B. Brumbaugh, V. A. Avanzato, R. Rosenke, P. W. Hanley, G. Saturday, D. Scott, E. R. Fischer, E. de Wit, Respiratory disease in rhesus macaques inoculated with SARS-CoV-2. *Nature* **585**, 268–272 (2020).
27. H. Zheng, H. Li, L. Guo, Y. Liang, J. Li, X. Wang, Y. Hu, L. Wang, Y. Liao, F. Yang, Y. Li, S. Fan, D. Li, P. Cui, Q. Wang, H. Shi, Y. Chen, Z. Yang, J. Yang, D. Shen, W. Cun, X. Zhou, X. Dong, Y. Wang, Y. Chen, Q. Dai, W. Jin, Z. He, Q. Li, L. Liu, Virulence and pathogenesis of SARS-CoV-2 infection in rhesus macaques: A nonhuman primate model of COVID-19 progression. *PLoS Pathog.* **16**, e1008949 (2020).
28. V. J. Munster, M. Koopmans, N. van Doremalen, D. van Riel, E. de Wit, A NOVEL CORONAVIRUS EMERGING IN CHINA - key questions for impact assessment. *N. Engl. J. Med.* **382**, 692–694 (2020).
29. R. Eccles, Pathophysiology of nasal symptoms. *Am. J. Rhinol.* **14**, 335–338 (2000).
30. B. Winther, J. M. Gwaltney Jr., N. Mygind, J. O. Hendley, Viral-induced rhinitis. *Am. J. Rhinol.* **12**, 17–20 (1998).
31. A. Akerlund, L. Greiff, M. Andersson, M. Bende, U. Alkner, C. G. Persson, Mucosal exudation of fibrinogen in coronavirus-induced common colds. *Acta Otolaryngol.* **113**, 642–648 (1993).
32. B. Pastorino, F. Touret, M. Gilles, X. de Lamballerie, R. N. Charrel, Prolonged infectivity of SARS-CoV-2 in fomites. *Emerg. Infect. Dis.* **26**, 2256–2257 (2020).
33. P. Venkatesan, The changing demographics of COVID-19. *Lancet Respir. Med.* **8**, e95 (2020).
34. D. Zhou, W. Dejnirattisai, P. Supasa, C. Liu, A. J. Mentzer, H. M. Ginn, Y. Zhao, H. M. E. Duyvesteyn, A. Tuekprakhon, R. Nutalai, B. Wang, G. C. Paesen, C. Lopez-Camacho, J. Slon-Campos, B. Hallis, N. Coombes, K. Bewley, S. Charlton, T. S. Walter, D. Skelly, S. F. Lumley, C. Dold, R. Levin, T. Dong, A. J. Pollard, J. C. Knight, D. Crook, T. Lambe, E. Clutterbuck, S. Bibi, A. Flaxman, M. Bittaye, S. Belij-Rammerstorfer, S. Gilbert, W. James, M. W. Carroll, P. Klenerman, E. Barnes, S. J. Dunachie, E. E. Fry, J. Mongkolsapaya, J. Ren, D. I. Stuart, G. R. Screaton, Evidence of escape of SARS-CoV-2 variant B.1.351 from natural and vaccine-induced sera. *Cell* **184**, 2348–2361.e6 (2021).
35. S. A. Madhi, V. Baillie, C. L. Cutland, M. Voysey, A. L. Koen, L. Fairlie, S. D. Padayachee, K. Dheda, S. L. Barnabas, Q. E. Bhorat, C. Briner, G. Kwatra, K. Ahmed, P. Aley, S. Bhikha, J. N. Bhiman, A. E. Bhorat, J. du Plessis, A. Esmail, M. Groenewald, E. Horne, S.-H. Hwa, A. Jose, T. Lambe, M. Laubscher, M. Malahleha, M. Masenya, M. Masilela, S. M. Kenzie, K. Molapo, A. Moultrie, S. Oelofse, F. Patel, S. Pillay, S. Rhead, H. Rodell, L. Rossouw, C. Taoushanis, H. Tegally, A. Thombayil, S. van Eck, C. K. Wibmer, N. M. Durham, E. J. Kelly, T. L. Villafana, S. Gilbert, A. J. Pollard, T. de Oliveira, P. L. Moore, A. Sigal, A. Izu; NGS-SA Group; Wits-VIDA COVID Group, Efficacy of the ChAdOx1 nCoV-19 Covid-19 Vaccine against the B.1.351 Variant. *N. Engl. J. Med.* **384**, 1885–1898 (2021).
36. L. J. Abu-Raddad, H. Chemaitelly, A. A. Butt, National Study Group for COVID-19 Vaccination, Effectiveness of the BNT162b2 Covid-19 Vaccine against the B.1.1.7 and B.1.351 Variants. *N. Engl. J. Med.* **385**, 187–189 (2021).
37. C. K. Yinda, J. R. Port, T. Bushmaker, R. J. Fischer, J. E. Schulz, M. G. Holbrook, C. Shaia, E. de Wit, N. van Doremalen, V. J. Munster, Prior aerosol infection with lineage A SARS-CoV-2 variant protects hamsters from disease, but not reinfection with B.1.351 SARS-CoV-2 variant. *Emerg. Microb. Infect.* **10**, 1284–1292 (2021).
38. S. Fukushi, T. Mizutani, M. Saijo, S. Matsuyama, N. Miyajima, F. Taguchi, S. Itamura, I. Kurane, S. Morikawa, Vesicular stomatitis virus pseudotyped with severe acute respiratory syndrome coronavirus spike protein. *J. Gen. Virol.* **86**, 2269–2274 (2005).
39. M. Kawase, K. Shirato, S. Matsuyama, F. Taguchi, Protease-mediated entry via the endosome of human coronavirus 229E. *J. Virol.* **83**, 712–721 (2009).
40. V. M. Corman, O. Landt, M. Kaiser, R. Molenkamp, A. Meijer, D. K. W. Chu, T. Bleicker, S. Brünink, J. Schneider, M. L. Schmidt, D. G. J. C. Mulders, B. L. Haagmans, B. van der Veer, S. van den Brink, L. Wijsman, G. Goderski, J.-L. Romette, J. Ellis, M. Zambon, M. Peiris, H. Goossens, C. Reusken, M. P. G. Koopmans, C. Drosten, Detection of 2019 novel coronavirus (2019-nCoV) by real-time RT-PCR. *Euro Surveill.* **25**, 2000045 (2020).
41. R. Wolfel, V. M. Corman, W. Guggemos, M. Seilmaier, S. Zange, M. A. Müller, D. Niemeyer, T. C. Jones, P. Vollmar, C. Rothe, M. Hoelscher, T. Bleicker, S. Brünink, J. Schneider, R. Ehmann, K. Zwirgmaier, C. Drosten, C. Wendtner, Virological assessment of hospitalized patients with COVID-2019. *Nature* **581**, 465–469 (2020).
42. M. Martin, Cutadapt removes adapter sequences from high-throughput sequencing reads. *EMBnet J.* **17**, 10–12 (2011).
43. A. McKenna, M. Hanna, E. Banks, A. Sivachenko, K. Cibulskis, A. Kernytsky, K. Garimella, D. Altshuler, S. Gabriel, M. Daly, M.-A. DePristo, The Genome Analysis Toolkit: A MapReduce framework for analyzing next-generation DNA sequencing data. *Genome Res.* **20**, 1297–1303 (2010).
44. E. Haddock, F. Feldmann, W. L. Shupert, H. Feldmann, Inactivation of SARS-CoV-2 laboratory specimens. *Am. J. Trop. Med. Hyg.* **104**, 2195–2198 (2021).

Acknowledgments: We thank T. Thomas, R. Rosenke, and D. Long for assistance with histology; RMBV animal care staff for taking care of the animals; J. Schulz, E. Haddock, S. Ricklefs, K. Barbian, K. Cordova, M. Woods, and C. Shaia for technical assistance; A. Mora for assistance with the figures; M. Ranjan and K. Stemple for assistance in acquiring the VOC isolates; and S. Rashid at BEI Resources for advice on culturing conditions for the VOC isolates. We thank C. Bushmaker (Marcus Daily Memorial Hospital) for providing the clinical specimen resulting in the D614G isolate used here, and A. Pekosz at Johns Hopkins University Bloomberg School of Public Health for the B.1.351 isolate. SARS-CoV-2 isolate hCoV-19/England/204820464/2020, NR-54000, contributed by B. Hallis, was obtained through BEI Resources, NIAID, NIH. **Funding:** This study was supported by the Intramural Research Program of NIAID, NIH. **Author contributions:** Conceptualization: V.J.M. and E.d.W.; investigation: V.J.M., M.F., M.S., C.K.Y., B.N.W., F.F., L.P.-P., J.S., B.B., M.G.H., D.R.A., A.O., P.W.H., B.J.S., J.L., S.L.A., C.M., N.v.D., G.S., and E.d.W.; writing (original draft): V.J.M. and E.d.W.; writing (review and editing): all authors. **Competing interests:** The authors declare that they have no competing interests. **Data and materials availability:** All data included in this manuscript have been deposited in Figshare at <https://doi.org/10.6084/m9.figshare.14551011.v1>. Sequences have been deposited in NCBI under BioProject accession number PRJNA727012.

Submitted 7 May 2021

Accepted 1 September 2021

Published 22 October 2021

10.1126/sciadv.abj3627

Citation: V. J. Munster, M. Flagg, M. Singh, C. K. Yinda, B. N. Williamson, F. Feldmann, L. Pérez-Pérez, J. Schulz, B. Brumbaugh, M. G. Holbrook, D. R. Adney, A. Okumura, P. W. Hanley, B. J. Smith, J. Lovaglio, S. L. Anzick, C. Martens, N. van Doremalen, G. Saturday, E. de Wit, Subtle differences in the pathogenicity of SARS-CoV-2 variants of concern B.1.1.7 and B.1.351 in rhesus macaques. *Sci. Adv.* **7**, eabj3627 (2021).